Retrieval of sizes and total masses of particles in volcanic clouds using AVHRR bands 4 and 5

Shiming Wen and William I. Rose

Department of Geological Engineering, Geology and Geophysics, Michigan Technological University, Houghton

Abstract. The advanced very high resolution radiometer (AVHRR) sensor on polar orbiting NOAA satellites can discriminate between volcanic clouds and meteorological clouds using two-band data in the thermal infrared. This paper is aimed at developing a retrieval of the particle sizes, optical depth, and total masses of particles from AVHRR two-band data of volcanic clouds. Radiative transfer calculations are used with a semi-transparent cloud model that is based on assumptions of spherical particle shape, a homogeneous underlying surface, and a simple thin cloud parallel to the surface. The model is applied to observed AVHRR data from a 13-hour old drifting cloud from the August 19, 1992, eruption of Crater Peak/Spurr Volcano, Alaska. The AVHRR data fit in the range of results calculated by the model, which supports its credibility. According to the model results, the average of effective particle radius in the test frame of this cloud is in the range of 2 to 2.5 μm, the optical depth at 12 μm is about 0.60 - 0.65. The total estimated mass of ash in the air amounts to 0.24 - 0.31 x 10^6 tons, which is about 0.7-0.9% of the mass measured in the ashfall blanket. Sensitivity tests show that the mass estimate is more sensitive to the assumed ash size distribution than it is to the ash composition.

Introduction

Measuring the size and burden of silicates and other components in volcanic clouds is of interest to those studying volcano-atmosphere interactions (Table 1). Weather satellites have been a useful way to track drifting volcanic clouds [*Hanstrum and Watson*, 1983; *Sawada*, 1987], and two-band processing of thermal infrared data from weather satellites has allowed for the discrimination of volcanic and meteorological clouds [*Prata*,1989a; *Holasek and Rose*, 1991]. The explanation of the cause of infrared two-band discrimination and volcanic clouds has been discussed by *Prata* [1989a, 1989b], *Holasek and Rose* [1991], and *Schneider and Rose* [1993] and is the result of scattering and absorption of thermal emission from matter underneath the volcanic cloud by the cloud itself. In this paper we develop a model of radiative transfer to attempt to retrieve the particle sizes and masses of particles in drifting volcanic clouds. The model builds on work of *Prata* [1989b] on volcanic clouds, on methodology published by *Yamanouchi et al.* [1987], and on cloud retrieval methods of *Lin and Coakley* [1993]. We compare our method with actual data on the Crater Peak/-Spurr eruption of August 19, 1992, to begin to evaluate the model and to discuss some of the uncertainties and applications.

Basic Theory

Radiative transfer calculations have been used to develop two-band models for retrieving the optical parameters of clouds, such as particle sizes, emissivity, transmissivity, and cloud cover, because radiance attenuation through the atmosphere depends on geometrical and optical properties of the clouds in the process of radiative transfer. The observed radiances by a satellite-based remote sensor through a semitransparent cloud is composed of two parts, radiance from the clouds and from the underlying surface. Generally, if the fraction of partial cloud cover in a field of view is taken into account [*Coakley*, 1983; *Lin and Coakley*, 1993], a linear model is valid under the following assumptions: (1) the cloud approximates a planar homogeneous cloud layer parallel to the surface (or a single-layer cloud system); (2) the background surface is homogenous; and (3) the atmosphere above the cloud and between the surface and the cloud are clear windows. In this case the observed radiance I_i in a narrow band i centered at wavelength λ_i is given by the following equation:

$$I_i = (1 - A_c)B(T_s) + A_c(\epsilon_i B(T_c) + t_i B(T_s)) \qquad (1)$$

where T_s is the brightness temperatures of the surface, T_c the temperature of the top of the cloud, B the Planck function, A_c the fraction of the clouds in the field of view, ϵ_i the emissivity, and t_i transmissivity of the clouds. The pixels are partially covered by clouds if A_c is less than 1. If the clouds are optically thick and completely overcast (ϵ_i=constant and

Table 1. Need for Satellite Data on Volcanic Silicates in Atmosphere

Research Foci Requiring Data on Masses and Sizes of Volcanic Cloud Silicates

Volume of erupted magma
    measure amounts of fine particles
    maps of ash and ash loading patterns in plumes
Gas volume versus magma volume
    petrologic methods of estimating SO_2: "excess sulfur"
    entrainment of H_2O: source of stratospheric water
Fallout of fine particles
    particle size distributions in drifting volcanic clouds
    fallout models
    mechanisms of fallout
Interactions between silicates and eruption cloud gases
    self-limiting effects: scavenging of chlorine and sulfur
    separation of silicates and sulfate aerosols
    comparisons to TOMS SO_2 measurements
Cloud height and eruption rate
    interpretation of eruption activity
    evaluation of column models
Drifting volcanic clouds
    radiative forcing to the atmosphere
    input into trajectory models
    hazardous aircraft encounters

$A_c=1$), the measured radiance I_i approximately equals $B(T_c)$. On the other hand, for a partially transparent cloud layer overlying a warm surface ($B(T_s) >> B(T_c)$), the radiance (I_i) approaches $t_iB(T_s)$ as ε_i, a measure of the transparency, approaches 0.

To obtain the theoretical radiance defined in equation (1), the radiative transfer calculation has to be processed because of unknown emissivity and transmissivity at different wavelengths. A monochromatic radiance under a scattering plane-parallel atmosphere assumption is associated with optical and physical parameters of the media through the radiative transfer equation [*Chandrasekhar*, 1960]. Using the means of Eddington's approximation to compute radiative transfer equation under proper cloud boundary conditions [*Liou*, 1992; *Shettle and Weinman*, 1970], the reflectivity (r) (the proportion of reflective flux at the top of the atmosphere to the incident flux) and the transmissivity (t) (the proportion of transmitted flux to incident flux) through the cloud layer are known functions of cloud optical depth (τ), the single-scattering albedo (ω), and the asymmetric parameter (g), i.e., $r=r(\tau,\omega,g)$, $t=t(\tau,\omega,g)$, and $\varepsilon=1-r-t$.

Temperature Difference Model

Prata [1989b], *Wu* [1987], and *Yamanouchi et al.* [1987] applied the temperature difference method to retrieve weather cloud parameters for complete cloud cover. The radiative calculation for the temperature difference method is a special case of equation (1) under the assumption $A_c=1$. The study frame selected (see below, Figure 1) is located over the center of the cloud image, and most of the pixels except those which are located at the edge of the cloud can be reasonably considered as complete cloud cover but still partially semitransparent.

Band 4 (10.3 -11.3 μm) and band 5 (11.5 - 12.5 μm) of the advanced very high resolution radiometer (AVHRR) are used in our temperature difference model, because the temperature difference of band 4 and band 5 $(T_4 - T_5)$ is a fairly reliable criterion used to distinguish meteorological clouds and volcanic clouds. When a volcanic cloud exists, $T_4 - T_5$ is usually < 0, otherwise $T_4 - T_5 > 0$ [*Prata*, 1989a; *Schneider et al.*, 1993].

The purpose of the temperature difference model (TDM) proposed here is to estimate the mass of particles in volcanic clouds. Two parameters, particle radius and optical depth, are essential in this model. The radiative transfer model is based on the following assumptions: (1) the shape of the volcanic particles is spherical, therefore Mie theory can be used to calculate extinction cross section (σ_e), asymmetric parameter (g), and the single-scattering albedo (ω) for a known refractive index (which depends on wavelength and composition) and particle radius; (2) the particle size distribution, $n(r)$, is uniform and monodisperse within each pixel; and (3) the volcanic clouds are continuous, i.e., $A_c=1$. Based on assumption (3), equation (1) can be expressed as

$$I_i=(1-R_i(r_e,\tau_c))B(T_c)+t_i(r_e,\tau_c)(B(T_s)-B(T_c)) \tag{2}$$

where r_e is the effective radius of the spherical particle for given size distribution $n(r)$, i.e.,

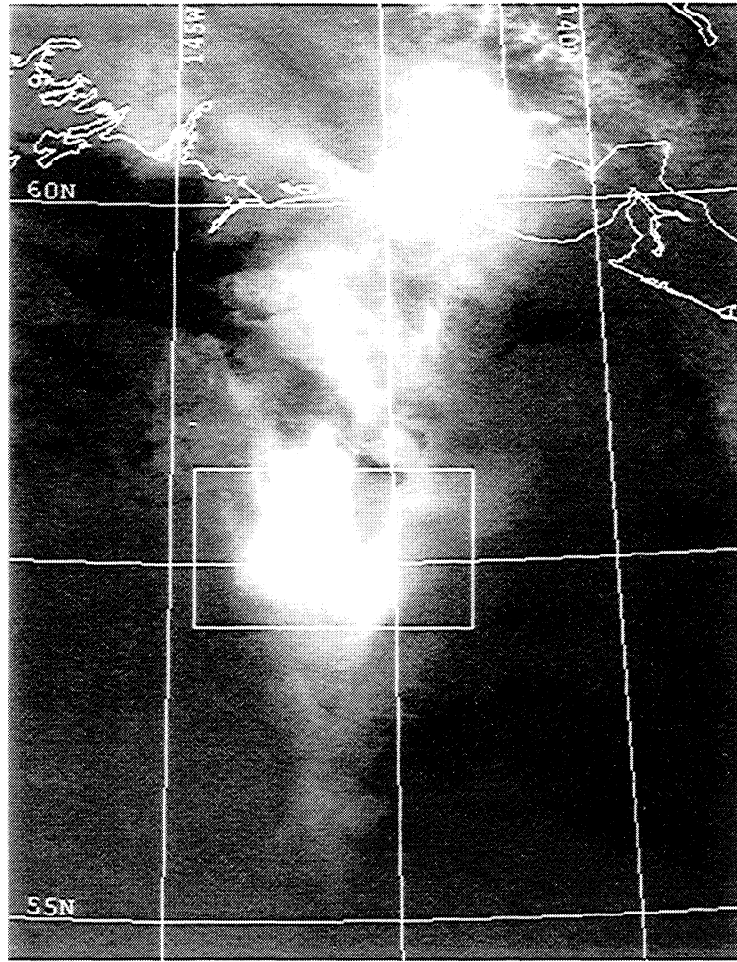$$r_e=\frac{\int \pi r^3 n(r)dr}{\int \pi r^2 n(r)dr} \tag{3}$$

Figure 1. The advanced very high resolution radiometer (AVHRR) band 4 image of the image of the Crater Peak/Spurr eruption cloud, August 19, 1992, 1338 GMT. The rectangle outlined is the study frame, with an area of about 165 km x 110 km. In the central part of the cloud shown, A_c=1 for all pixels, but at the edges, sometimes this is not true.

and τ_c is the optical depth of the cloud, defined by

$$\tau_c = L \cdot \int Q_{ext} \pi r^2 n(r) dr \qquad (4)$$

where L is the geometric thickness of the clouds, Q_{ext} is the efficiency extinction factor calculated by Mie theory, and $\sigma_e = \pi r^2 Q_{ext}$ is extinction cross section.

Once the simultaneous pairs of radiance (I_i, I_j) are calculated for varying r_e and τ_c, the corresponding brightness temperature pairs for the two AVHRR channels (T_i, T_j) can be obtained by the rearranged version of the Planck's formula:

$$T_i = \frac{1.43879 \times 10^4}{\lambda_i \ln([3.74151 \times 10^8 \lambda_i^{-5} / \pi I_i] + 1)} \qquad (5)$$

where λ_i is wavelength in microns.

Theoretical calculations based on the model are shown in Figure 1, where the solid lines represent the effective radius

of volcanic ash particles and dashed lines represent the 10.8-μm (band 4) optical depth of the cloud. The model reveals a nonlinear relationship of temperature difference with brightness temperature due to the nonlinear relation of optical depth with wavelengths. The theoretical calculation shows that the most negative temperature difference (|TD|) of band 4 and band 5 linearly depends on the temperature difference of the cloud top and the surface (T_s - T_c), i.e., when T_s -T_c increase, |TD| will linearly increase. If the surface temperature T_s is 273 K and the cloud top is 213 K (the conditions of our test data set), |TD| cannot be lower than -30°C, and the brightness temperature corresponding to |TD| is about 227 K. The characteristics of negative temperature difference will disappear completely if the particle size is greater than 5 μm (see Figure 2).

In Figure 2, let $S(r_e)$ be a variable that records the size of the area embraced by the straight line which represents the appearance of 0° temperature difference and the curved line which represents the change of the temperature pairs (T_4, T_4-T_5) along with a varying degree of transparency at different effective radii r_e. Thus S is a function of r_e. A plot of normalized S (maximum S is assigned to 1) versus the
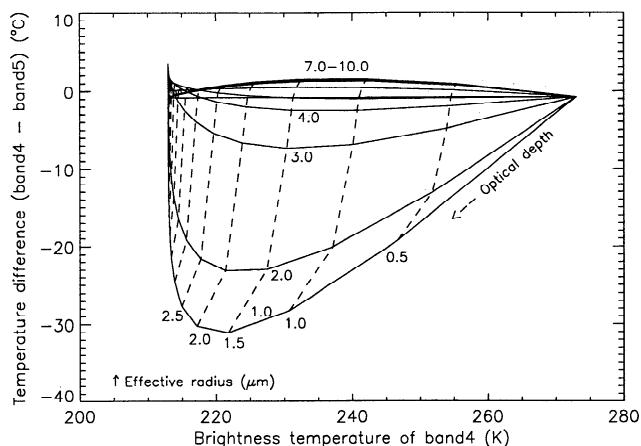
Figure 2. Two-band temperature difference model at 10.8 μm and 12 μm. The near horizontal solid curves represent different effective radii, and the near vertical dashed curves represent the dependence of optical depth at 10.8 μm with particle radius.

particle radius (r_e) is shown in Figure 3. $S(r_e)$ is a parameter that represents the retrieval sensitivity of the effective radius. If S is a monotonic function, then the observed temperature pairs $(T_4, T_4 - T_5)$ can be uniquely related to effective radius and optical depth pairs (r_e, τ_c). In our example (Figure 3), $S(r_e)$ is a monotonically decreasing function in this interval from 0.8 to 4.3 μm.

Study Case

As an initial test for our model we examined volcanic cloud data taken from the August 19, 1992, Crater Peak/-Spurr eruption. Nine digital images of AVHRR were received from the NOAA 11 and 12 polar-orbiting satellites. Previous study [*Schneider et al.*, 1993] indicates that the images taken early in the eruption are apparently rich in water droplets and/or ice of large particle size. This makes the spectral signal similar to a meteorological cloud.
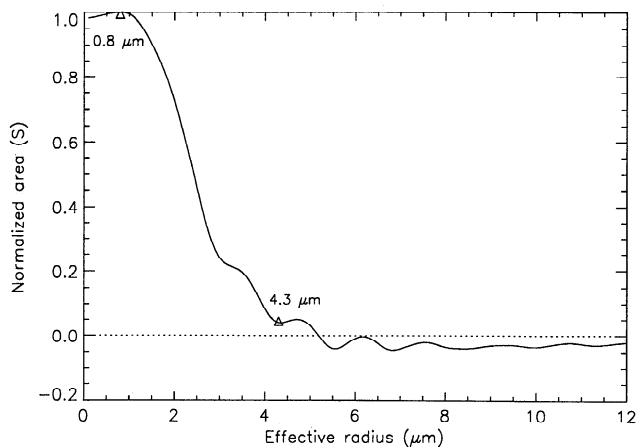

Figure 3. Effective radius and normalized negative temperature domain areas. The normalized areas reflect the sensitivity of the temperature difference model to the effective radius.

However, when the drifting volcanic clouds dry out and the particle size becomes small during transport and dispersion, the clouds take on spectral properties dominated by fine volcanic ash. For the purpose of this study, the selected data were taken at 1338 GMT on August 19, 1992, about 13 hours after the onset of the eruption and nine hours after it ended. At this point the cloud was located over the Gulf of Alaska, more than 300 km from the Spurr Volcano. We used a sample frame of 1.1 km resolution local area coverage (LAC) data of cloud surface temperatures of band 4 and band 5. In the sample frame, composed of 150 × 100 pixels, covering an area of about 18150 km^2, the volcanic clouds overlapped low-level meteorological clouds (Figure 1).

Parameter Selection

For this study, we do not have refractive index measurements for the Spurr ash. We assume that the volcanic clouds contain only volcanic ash and we use refractive index data for other ash samples and volcanic materials obtained by *Volz* [1973] and *Pollack et al.* [1973]. The six samples provide a good variety of volcanic ash types with crystalline andesite, crystalline basalt, glassy basalt, and glassy rhyolites (Table 2). The composition of the Crater Peak/Spurr eruption is andesite, similar to sample 1; therefore we focus on the refractive index of sample 1 and test the sensitivity of the refractive index by comparing results using the other samples.

The cloud top temperature (T_c) is chosen at 213 K, which is obtained from the brightness temperature of the coldest part of an earlier AVHRR image of the same volcanic clouds, where the absolute temperature difference between band 4 and band 5 is less than 0.5°C. The image with optically opaque portion in the 10- to 12-μm range is about eight hours before 1338 GMT and five hours after the onset of the eruption. The surface temperature (T_s) used was 273 K, determined from the band 4 and band 5 brightness temperatures for areas that surround the volcanic cloud in the AVHRR images, which are free of meteorological clouds, except for the homogeneous low deck of clouds that underlies the volcanic cloud.

Retrieval of Particle Sizes and Optical Depths

Figure 4 shows results obtained from actual pixels in the sample frame superimposed on the calculated curves of Figure 2. Most of the points in the frame cluster are between particle sizes of 1 and 4 μm. To understand the spatial distribution of effective radiance, 20 theoretical curves from 0.8 to 5 μm with equal increments were calculated to analyze the AVHRR data in more detail. The minimum effective radius is selected to be 0.8 μm rather than 0 because of the existence of multiple solutions of our model for radius less than 0.8 μm (note the nondecreasing function $S(r_e)$ fraction of Figure 3). An effective radius is assigned to a pixel (a point in Figure 4) if the standard for the effective radius curve is the closest one among the 20 curves to the point of pixel. When the points are out of the retrieving size range of the model (less than 3% of all the pixels), those points where $T_4 - T_5 > 0$ °C are not used since they are not considered to be volcanic cloud pixels, and an index effective radius of "0" is assigned; others, where $T_4 - T_5 < 0$ and the point plots below the smallest radius curve (none in this sample frame), are arbitrarily assigned to be the smallest effective radius. The frequency distribution shows that the

Table 2. Refractive Index of Different Samples

Sample Description	Band 4, 10.3-11.3 μm		Band 5, 11.5-12.5 μm		Source
	Real	Imaginary	Real	Imaginary	
(1) Andesite, 54.12% SiO$_2$	2.0534	0.60897	1.8392	0.13786	Pollack et al. [1973]
(2) Basalt, 53.25% SiO$_2$	2.1848	0.48812	1.9051	0.14670	Pollack et al. [1973]
(3) Basaltic glass, 53.45% SiO$_2$	2.1241	0.71211	2.0129	0.24037	Pollack et al. [1973]
(4) Obsidian-little glass, Mt. California, rhyolite, 73.45% SiO$_2$	2.0085	0.27476	1.7281	0.18407	Pollack et al. [1973]
(5) Obsidian-Lake County Oregon, rhyolite, 76.20% SiO$_2$	2.0268	0.27882	1.7410	0.18462	Pollack et al. [1973]
(6) Volcanic dust: two samples are averaged. The andesitic Irazu ash sampled during ashfall is dark grey with feldspar, and the Hawaii sample was lightly weathered vesicular basaltic glass.	1.9700	0.3700	1.8000	0.18000	Volz [1973]

mean radius and standard deviation are 2.80 and .56 μm, respectively (Figure 5). Mapping effective radii allows examination of the spatial distribution of particle size (Figure 6). The contour map shows that the effective particle sizes in the frame vary from 2.5 and 3 μm at the center, to between 3 and 4 μm in the west, and to between 2.5 and 2.0 μm in the east. There is a dramatic difference in particle size at the east and west edges of the frame (also the edges of the clouds), and the center is relatively homogenous (also the center of clouds). This variation could be due to changes in cloud altitude with dispersal as volcanic ash particles are being fractionated. A possible explanation consistent with the observed data is that the eastern edge of the cloud is higher and has moved faster than the western edge. It is also
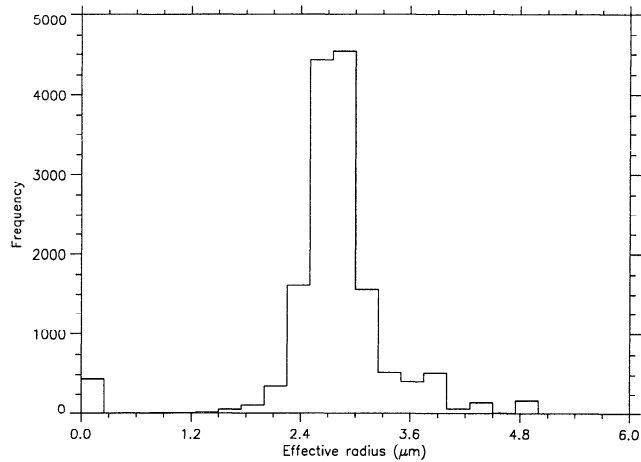

Figure 5. Frequency distribution of effective radius for the pixels plotted in Figure 4. The population plotted in the "0" radius region are the pixels where T_4-T_5>0· C.

possible that at the edges of the cloud, the assumption of continuous coverage is violated, which gives us spurious results. Another possibility is that the optically thin edges of the volcanic cloud overlap a lower-level water cloud which skews the R_e contours.

The spatial distribution of optical depths of band 4 is shown in Figure 7, where 20 curves of optical depth with increments of 0.1 are calculated for retrieval. The optical depth in the sample test frame varies from 0.1 to 1.25, the mean value is 0.66 and the standard deviation is 0.28. The largest values of optical depth appear at the center of the clouds, and the smallest ones are at the cloud edges.

Estimation of the Total Mass

Using a density of 2.6 g cm^{-3} [*Neal et al.*, 1994] for the volcanic particles, the total mass of the frame is the accumulation of pixel-scale mass, i.e.,
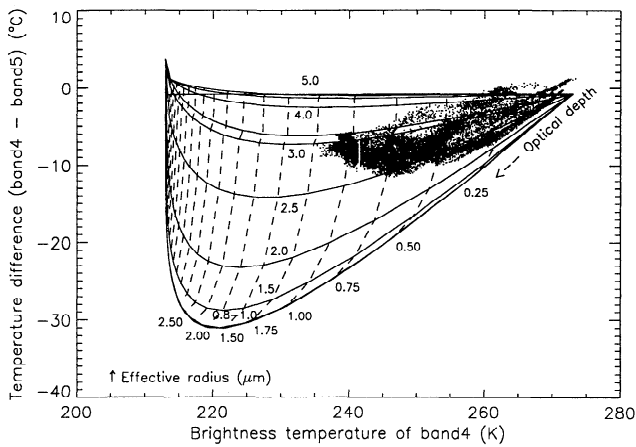

Figure 4. Simulated temperature pairs, the temperature differences (band 4 at 10.8 μm-band 5 at 12 μm) and brightness temperature differences at 10.8 μm, as a function of effective radius and the optical depth (identical conditions, as those shown in Figure 2), compared with the observed AVHRR data of the frame shown in Figure 1. The small dots in the plot represent individual pixel values.
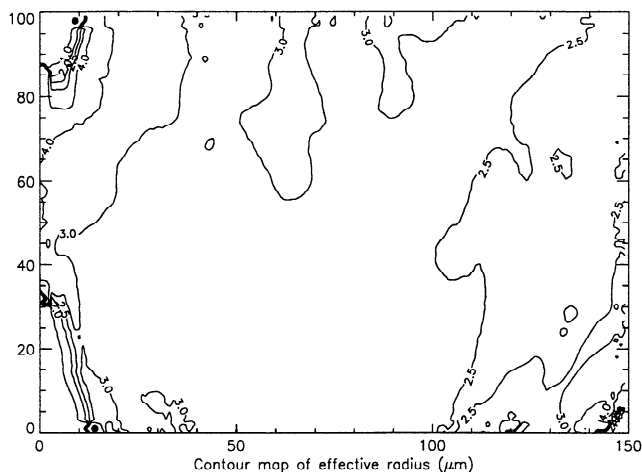
Figure 6. Contour map, for the sample frame of Figure 1, of the effective radius in pixel-scale retrieval. The numbers in the contour map are the effective radius in microns. Numbers on the axes indicate distances along the edge of 1.1-km pixels.

$$M_{total} = \sum_{n=1}^{100} \sum_{m=1}^{150} L^{(n,m)} S \rho \int \frac{4}{3} \pi r^3 n(r) dr \qquad (6)$$

$$= \sum_{n=1}^{100} \sum_{m=1}^{150} 1.21 \times \frac{4}{3} \rho r_r^{(n,m)} \tau^{(n,m)} \frac{\int \pi r^2 n(r) dr}{\int Q_{ext} \pi r^2 n(r) dr} \qquad (ton)$$

where ρ(g cm^{-3}) is particle density, $r_e^{(n,m)}$ (μm) and $\tau^{(n,m)}$ are retrieval effective radius and optical depth of pixel (n,m), respectively. $L^{(n,m)}$ is geometric thickness of pixel (n,m) and S is the area of each pixel. If the particle distribution $n(r)$ reduces to uniform distribution, i.e., $n(r)=1$, then the inner term of the above sum simply becomes $1.21 \times 4/3 \times \rho r_e^{(n,m)} \tau^{(n,m)} / Q_{ext}(r_e^{(n,m)})$, where $Q_{ext}(r_e^{(n,m)})$ is extinction efficiency factor at effective radius $r_e^{(n,m)}$.
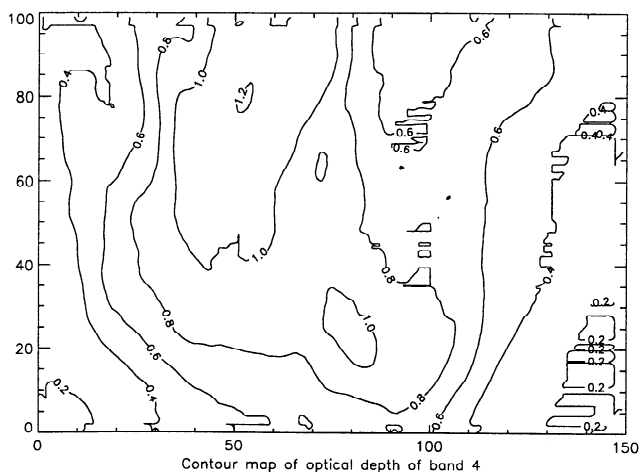

Figure 7. Contour map, as in Figure 6, of the optical depth at 10.8 μm (band 4).

Using the retrieval of $r_e^{(n,m)}$, $\tau^{(n,m)}$, and Q_{ext} discussed above, the total mass of volcanic ash in the sample frame is about 38,000 tons. By extending the result to the whole cloud (about 100,000 km^2 total area, see Figure 1), the total estimated mass in the air is about 0.2×10^6 t, which is about 0.56% of the total volcanic ash measured in the deposited ash blanket (36×10^6 t) [*Neal et al.*, 1994]. This means that over 99% of ash erupted was deposited in less than 13 hours. Similar studies of younger eruption clouds could provide more information about the rate at which the bulk of an ash cloud is deposited, although the two-band AVHRR method will not work well for ash with an effective radius greater than about 4 μm.

Since we have little direct information for the size distribution of ash in the study cloud, the above estimation is based on the assumption of uniform size distribution. In the next section, however, we will show that the total mass estimates are not significantly different for several possible nonuniform size distributions.

Sensitivity Study of Parameter Selections

The temperature difference model for a homogenous parallel cloud is strongly controlled by the refractive index of particles in the cloud (which is dependent on their chemical composition), environmental variables T_s and T_c, the shape of the particles, and the size distribution of particles. Uncertainties in any of these parameters will influence the accuracy of the retrieval. We did sensitivity studies of the model for variety of assumptions and parameter selections based on the selected cloud. Additional studies of other volcanic clouds are needed to validate the model and to determine the conditions which favor accurate retrievals.

Silicates and Sulfuric Acid Aerosols

By using refractive index data only for volcanic ash, we are assuming that silicates are the only kind of particle in the volcanic cloud. This is not true. Silicates (volcanic ash) and sulfuric acid aerosol particles are both found in volcanic ash clouds [*Rose et al.*, 1980; *Rose*, 1986; *Tabazedeh and Turco*, 1993]. *Prata* [1989a] showed that either silicates or sulfuric acid can produce negative apparent temperature differences. We used refractive index data for sulfuric acid aerosols [*Halperin and Murcray*, 1987] to calculate model results analogous to those for silicates, for a variety of dilutions of H$_2$SO$_4$. Results show that aerosol with >50% H$_2$SO$_4$ are indistinguishable from silicates with two-band AVHRR retrievals. The possible confusion of the two types of particles depends partly on the age of the volcanic cloud because ash is the dominant particle component of young ash clouds [*Rose et al.*, 1980; *Rose*, 1986] but is removed from the atmosphere relatively quickly, in days to months [*Turco et al.*, 1983; *Pinto et al.*, 1989], while volcanic sulfuric acid may persist in the atmosphere for several years [*Rampino et al.*, 1988; *Bernard and Rose*, 1990]. For the Spurr cloud we used in our study, silicates probably exceed sulfuric acid particles by orders of magnitude. After atmospheric residence times of a week or more, confusion between the two particle types would be more of an issue. We have begun to investigate whether three-band retrievals, involving band 3 of AVHRR (3.5 μm), can be used to distinguish between concentrated H$_2$SO$_4$ and silicate components. This may open
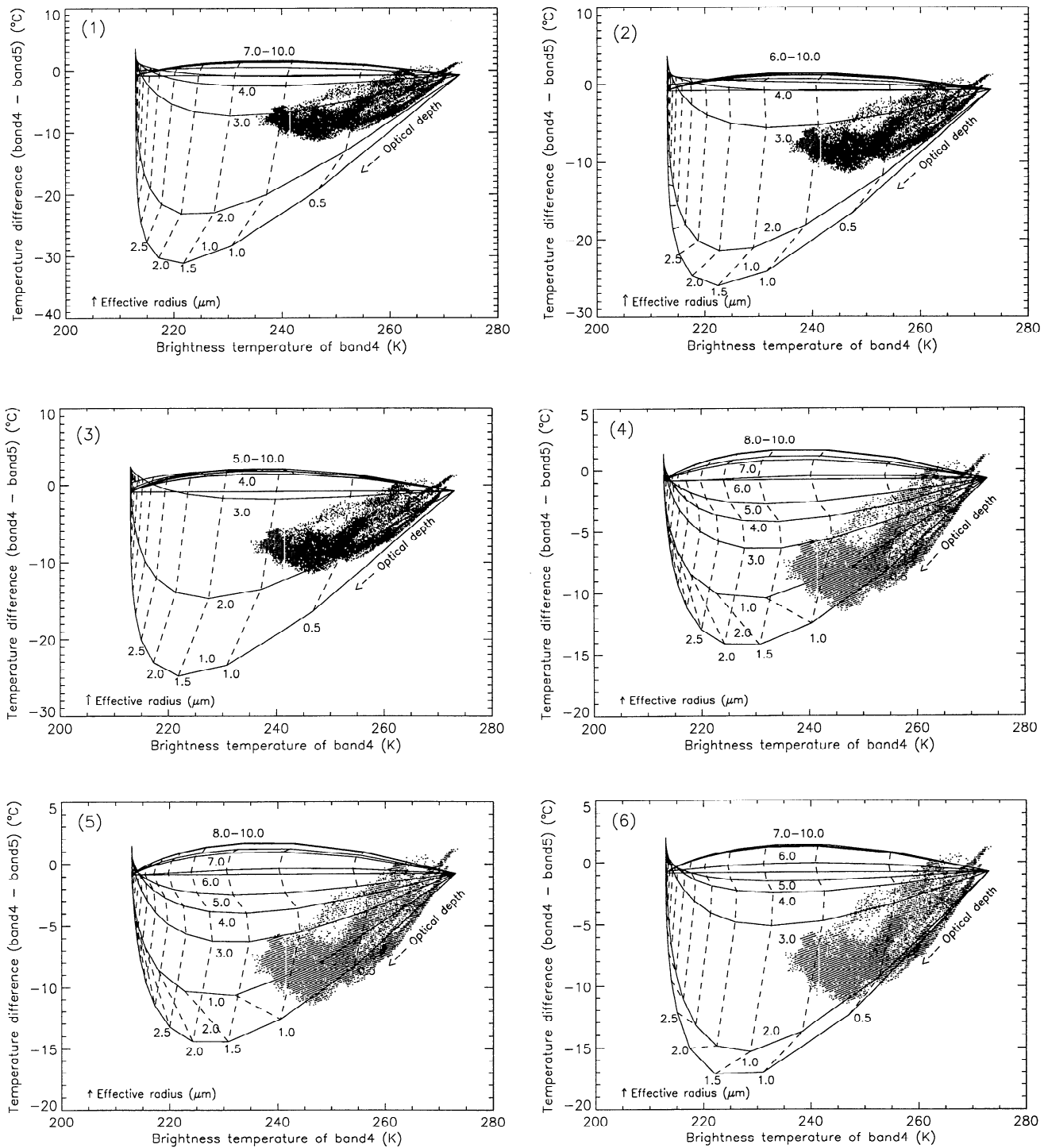
Figure 8. The comparison of models similar to Figure 4 testing the model sensitivity to different refractive indices. The numbers 1-6 in the figures correspond to the six samples and their refractive indices, listed in Table 2.

the range of retrievable sizes, but the intensity of band 3 radiation in nighttime AVHRR may not be sufficient. During the day it is useless due to reflected solar.

Uncertainty About Refractive Index of Volcanic Ash

To investigate the sensitivity of our model to uncertainties about refractive index of volcanic ash, we compared results

using the data from a variety of samples (Figure 8, Table 3). Some of the refractive index data (samples 4, 5, and 6) cause pixel points to fall outside of the fields of calculated results, and we interpret this to reflect a lack of similarity in composition for those samples to the Spurr ash. For the three samples that do match Spurr well, the effective radius determined ranges from 2.2 to 2.8 μm, the optical depth from

Table 3. Pixel-Scale Retrieval of Masses for Different Samples

Samples	Retrieving Particle Range, µm	Mean Effective Radius, µm	Mean Optical Depth	Estimated Mass Frame	Estimated Mass Cloud
1	0.8 - 5.2	2.8024	0.6647	37,999	209,000
2	1.0 - 5.0	2.6163	0.6890	36,236	200,000
3	0.9 - 3.6	2.1838	0.6215	30,516	168,000

0.62 to 0.68 and the mass in the frame from 30,000 to 38,000 t. It would obviously be desirable to have refractive index data on the Spurr ash, but the sensitivity of this uncertainty does not seem too serious at this initial stage of model development.

Size Distribution of Particles

The mass calculation is obviously dependent on the size distribution of particles (note the equations (3),(4), and (6)). The assumed uniform distribution is undoubtedly too simple to be reliable. For nonuniform size distributions, the efficiency factors are defined by the Mie single efficiency factors weighted by the area of particle cross section and the size distributions, i.e.

$$Q_f = \int_0^\infty \pi r^2 Q_f(\frac{2\pi r}{\lambda},m)\frac{dn(r)}{dr}dr/\int_0^\infty \pi r^2 \frac{dn(r)}{dr}dr \quad (7)$$

where Q_f is the Mie efficiency factor for extinction, scattering, or absorption; $n(r)$ is the size distribution of particles with radius r, and m is the refractive index for the particle composition. The asymmetric parameter is

$$\hat{g} = \int_0^\infty \pi r^2 Q_{sca}g(\frac{2\pi r}{\lambda},m)\frac{dn(r)}{dr}dr/\int_0^\infty \pi r^2 Q_{sca}\frac{dn(r)}{dr}dr \quad (8)$$
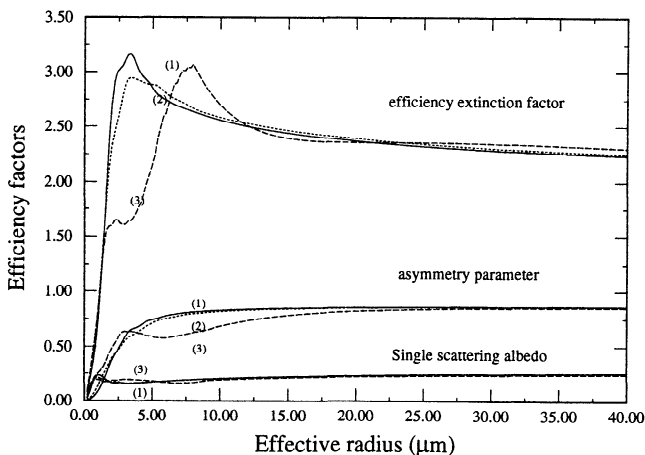

Figure 9. Relationship of effective radius and efficiency factors at 10.8 µm for different size distributions of particles. Number 1 (solid line) is associated with uniform distribution, number 2 (dotted line) with gamma, and number 3 (dashed line) with lognormal distribution.
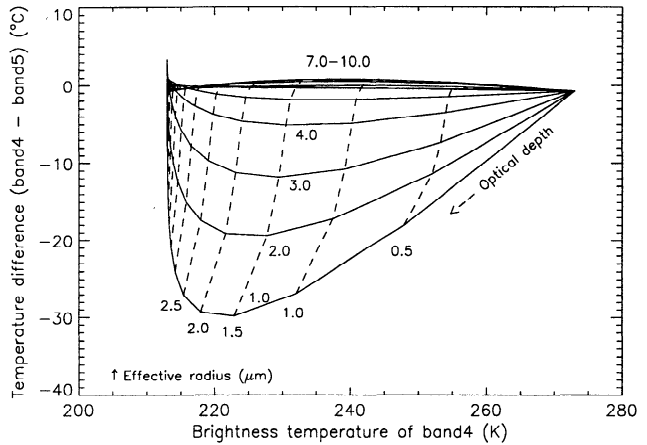

Figure 10. Two-band temperature difference model like Figure 2 but for gamma size distribution of particles.

where g is asymmetric parameter for single particle and Q_{sca} is Mie scattering efficiency factor. Two size distributions, gamma (usually used for water/ice clouds) and lognormal (possibly more appropriate for volcanic clouds), have been suggested by many authors based on experiments and measurements [*Prata*, 1989b; *Farlow et al.*, 1981]. Measurements of particles in the 1990 volcanic clouds of Mount Redoubt [*Hobbs et al.*, 1991] show volcanic dust with a lognormal size distribution and 0.74 standard deviation (σ) and 0.8-µm mean particle radius. We assume that σ is equal to 0.74 and the upper integral limit in equations (7) and (8)
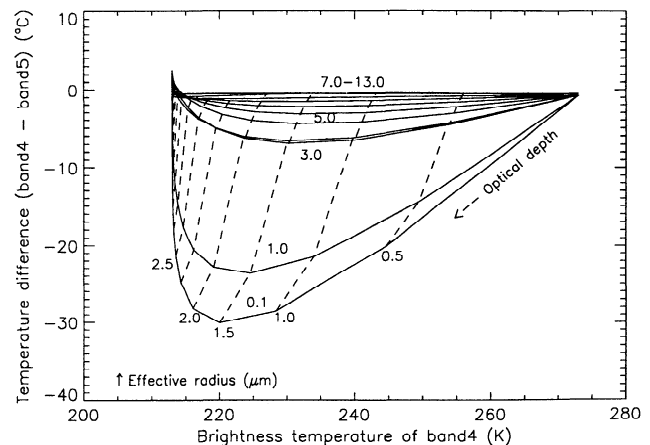

Figure 11. Two- band temperature difference model like Figure 2 but for lognormal size distribution of particles.

Table 4. Frame Scale Retrieval of Masses for Different Size Distributions

	Size Distribution								
	Uniform $n(r)=1$ at $r=r^e$			Gamma $n(r)=[(r_0/6)^7/6!]r^6\exp(-r_0r/6)$			Lognormal $\ln(r)=[1/(2\pi)^{1/2}\sigma r]\exp\{(\ln r-\mu)^2/2\sigma^2\}$		
Sample	1	2	3	1	2	3	1	2	3
				Retrieval					
Effective radius, μm	2.8024	2.6123	2.1804	3.0636	2.7557	2.113	2.3253	2.2534	1.8495
Mean radius, μm	2.8024	2.6123	2.1804	2.3828	2.1434	1.6420	0.7777	0.7537	0.6186
Optical depth	0.6647	0.6890	0.6862	0.6542	0.6692	0.6099	0.6539	0.6480	0.6062
Mass in a pixel, tons	2.5560	2.3167	1.8858	2.8937	2.6807	2.1666	3.8723	3.6076	2.9061
Mass in the frame, tons	37,192	33,710	27,440	42,106	39,007	31,526	56,346	52,494	44,287
Mass in the cloud, ton x 10^3	205	185	151	232	215	174	310	289	233
			Range of Effective Radius (μm) Which Can Be Uniquely Retrieved						
Minimum effective radius, μm	0.8	1.0	0.9	0.6	0.8	0.6	0.1	0.3	0.2
Maximum effective radius, μm	4.3	3.1	2.9	2.6	2.5	2.5	0.9	0.9	0.8
Maximum radius to get negative value of T4-T5	5.2	5.0	3.6	6.1	5.9	4.3	17.0	17.6	13.3

Note that r_e is effective radius, $r_0=(2/3)r_e$ the mode radius, $\mu=\ln(r_e)-2.5\sigma^2$ the mean of $\ln(r)$, and σ is the standard deviation of $\ln(r)$ which is chosen to be 0.74. In uniform distribution, mean=r_e and variance=0; in gamma, mean=$7r_e/9$, variance=$7r_e^2/81$; and in lognormal, mean=$e^r e_{r_e}$ and variance=$\exp(2\mu+\sigma^2)(\exp(\sigma^2)-1)$. Sample 1 is andesite, sample 2 is basalt, and sample 3 is glassy basalt.

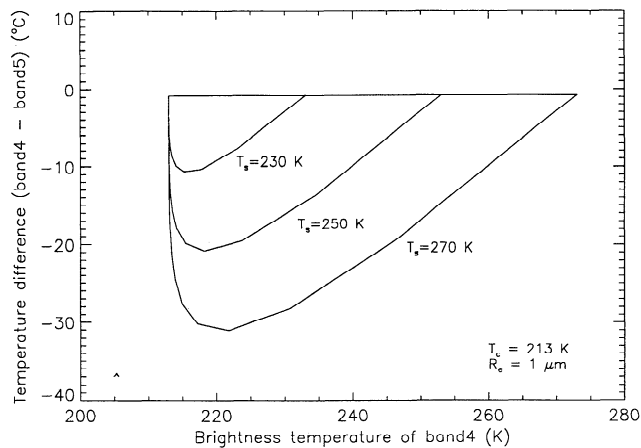**Figure 12.** Simplified plots of two-band temperature difference model like Figure 2 but with curves only for 1 μm uniform distribution at constant T_c(=213·C), showing the sensitivity to different underlying surface temperature (T_s).

is 50 μm. Figure 9 reveals the relationship of the effective radius to the efficiency factors under difference size distributions. It shows that scattering parameters have no significant difference when the effective radius is greater than 15 μm and that the scattering characteristics of gamma and uniform size distributions are quite similar, while lognormal distributions show a significant difference. Figures 10 and 11 show results of the temperature difference model for different size distributions. The figures show that different size distributions result in almost the same optical depths and most negative temperature differences but have a significantly different effective radius. Table 4 lists the comparison of the mass estimates based on different size distributions for the same sample frame discussed above. The mass estimates vary only slightly from the estimates based on a uniform distribution for some possible gamma and lognormal distributions which possibly span the ranges of volcanic clouds, based on a limited study of size distributions of particles by aircraft-based studies [*Rose et al.*, 1980; *Hobbs et al.*, 1991].

Table 4 suggests the following conclusion: (1) when the variance increases in size distributions, the estimated mass will increase as well; (2) when a lognormal distribution is chosen, an effective radius of 1.8 to 2.3 μm equals a lognormal average of particle radius of between 0.62 and 0.78 μm (which is smaller than the average radius (about 0.8 μm) of airborne measurements of the 1990 Mount Redoubt eruption cloud [*Hobbs et al.*, 1991]; (3) when three different refractive index values (1-3 in Table 2) are considered with a lognormal size distribution, the estimated mass in the whole cloud is in the range of 240 - 310×10³ t, i.e., about 0.7-0.9% of the total volcanic ash measured in the ash blanket. The sensitivity tests shown in Table 4 indicate that a better knowledge of size distribution is more important than the refractive index of the volcanic dust for an accurate mass estimate.

Temperature Difference Between the Volcanic Cloud and the Warmer Surface

The retrieval model we have developed is highly sensitive to the temperature difference $(T_s - T_c)$ between the warmer

surface (land, sea, or clouds) and the top of the volcanic cloud. We expect that $(T_s - T_c)$ values will be typically positive, because tropospheric temperatures decrease rapidly with height and drifting volcanic cloud particles will equilibrate with the temperature of surrounding air. However, the temperature of the surface can vary a lot, being highest on warm summer days in which there are no meteorological clouds $(T_s - T_c$ up to 100°C) and lowest on days when high cold clouds underlie the volcanic cloud or in winter at night when the surface temperatures may be much lower. Figure 12 is calculated under the same assumptions as a uniform distribution model but varying surface temperatures. It shows that when the surface temperature changes from 270 K to 230 K, the most negative temperature difference changes from about 30°C to 10°C. This effect helps explain why some AVHRR images are much more successful in mapping and discriminating volcanic clouds [*Schneider et al.*, 1994] than others [*Schneider and Rose*, 1993].

Conclusions and Discussions

Theoretical study and application of radiative transfer calculations to a volcanic cloud imaged by AVHRR can be used to retrieve the effective radius of volcanic ash particles and optical depths of clouds from AVHRR multispectral images. The major conclusions from this study are the following:

1. Volcanic clouds have negative brightness temperature differences (band 4 - band 5) only if they have a dominance of particles with a radius less than 5 μm.

2. Our model works best when there is a large difference between the temperature of the underlying surface and the volcanic cloud. The lowest temperature difference (band 4 - band 5) of the volcanic cloud is a linear function of the temperature difference between the underlying surface and the volcanic clouds $(T_s - T_c)$.

3. This method can be used to interpret volcanic clouds with a dominant effective radius between 0.8 and 4.3 μm for uniform size distribution, between 0.1 and 17 μm for lognormal size distribution.

4. The mean radius and the optical depths within the test frame of a 13-hour-old August 1992 Crater Peak/Spurr volcanic cloud are determined to be 2.8 and 0.66 μm, respectively, based on the two-band model. If lognormal size distribution is considered, the average of the particle radius is about 0.62 to 0.78 μm, the estimate of the mass of the volcanic cloud particles is about 42 - 56 × 10³ t in the frame and about 0.24 - 0.31×10⁶ t in the whole cloud, which is about 0.7 - 0.9% of the total volcanic ash measured in the deposited ash blanket (36x10⁶ t).

5. The mass estimate is more sensitive to the assumed ash size distribution than it is to the ash composition.

These results are valid only under the assumptions that the volcanic aerosols are spherical and that the volcanic cloud forms a well-defined homogeneous single layer in each pixel. In fact, volcanic ashes are usually nonspherical and irregular. It may be that equivalent spheres overestimate T_4-T_5 temperature differences for optically thin clouds composed of nonspherical particles. We are unable to calculate the exact T_4-T_5 temperature difference unless we address the shape effects. Some work has been done by *Drossart* [1990], which shows that spheres give one type of scattering, cubes another, and all other odd shapes give about the same type of

scattering which is different from that of spheres and cubes. Further work is needed to check the sensitivity of shapes even for the idealized sphere, cube, and cylinder shapes. Real volcanic clouds are not exactly homogenous either. In fact, the particle size distribution in Figure 6 suggests that the cloud in the frame is not a single parallel layer but instead probably has a range of altitudes. Therefore the accuracy of retrieval will be improved by a higher spatial resolution of the remote sensor. A smaller-sized pixel will reduce the effects of variable altitudes and the cloud within each pixel can be better approximated as a layer.

References

Bernard, A., and W.I. Rose, The injection of sulfuric acid aerosols in the stratosphere by El Chichón Volcano and its related hazards to the international air traffic, *Nat. Hazards*, *3*, 59-67, 1990.

Chandrasekhar, S., *Radiative Transfer*, 393 pp., Dover, Mineola, New York, 1960.

Coakley, J.A., Jr., Properties of multilayered cloud systems from satellite imagery, *J. Geophys. Res.*, *88*, 10,818-10,828, 1983.

Drossart, P., A statistical model for the scattering by irregular particles, *Astrophys. J.*, *361*, L29-L32, 1990.

Farlow, H.N., V.R. Oberbeck, K.G. Snetsinger, G.V. Ferry, G. Polkowski, and D.M. Hayes, Size distributions and mineralogy of ash particles in the stratosphere from eruptions of Mount St. Helens, *Science*, *211*, 832-834, 1981.

Halperin, B., and D.G. Murcray, Effect of volcanic aerosols on stratospheric radiance at wavelengths between 8 and 13 μm, *Appl. Opt.*, *26*(11), 2222-2235, 1987.

Hanstrum, B.N., and A.S. Watson, A case study of two eruptions of Mount Galunggung and an investigation of volcanic cloud characteristics using remote sensing techniques, *Aust. Meteorol. Mag.*, *31*, 171-177, 1983.

Hobbs, P.V., L.F. Radke, J.H. Lyons, R.J. Ferek, and D.J. Coffman, Airborne measurements of particle and gas emissions from the 1990 volcanic eruptions of Mount Redoubt, *J. Geophys. Res.*, *96*, 18,735-18,752, 1991.

Holasek, R.E., and W.I. Rose, Anatomy of 1986 Augustine Volcano eruptions as revealed by digital AVHRR satellite imagery, *Bull. Volcanol.*, *53*, 420-435, 1991.

Lin, X.J., and J.M. Coakley, Jr., Retrieval of properties for semitransparent clouds from multispectral infrared imagery data, *J. Geophys. Res.*, in press, 1993.

Liou, K.N., Radiation and cloud processes in the atmosphere, 487 pp., Oxford University Press, 1992.

Neal, C.A, R.G. McGimsey, C.A. Gardner, M.L. Harbin, and C.J. Nye, Tephra-fall from the 1992 eruptions of Crater Peak, Mount Spurr Volcano, AK: A preliminary report on distribution, stratigraphy and composition, *U.S. Geol. Surv. Bull.*, in press, 1994.

Pinto, J.P., R.P. Turco, and O.B. Toon, Self-limiting physical and chemical effects in volcanic eruption clouds, *J. of Geophys. Res.*, *94*, 11,165-11,174, 1989.

Pollack, J.B., O.B. Toon, and B.N. Khare, Optical properties of some terrestrial rocks and glasses, *Icarus*, *19*, 372-389, 1973.

Prata, A.J., Observations of volcanic ash clouds in 10-12 μm window using AVHRR/2 data, *Int. J. Remote Sens.*, *10*, 751-761, 1989a.

Prata, A.J., Infrared radiative transfer calculations for volcanic ash clouds, *Geophys. Res. Lett.*, *16*(11), 1293-1296, 1989b.

Rampino, M.R., S. Self, and R.B Stothers, Volcanic winters, *Ann. Rev. Earth Planet. Sci.*, *16*, 73-99, 1988.

Rose, W.I., Interaction of aircraft and explosive eruption clouds: A volcanologist's perspective, *AIAA Journal, 25*, 52-58, 1986.

Rose, W.I., R.L. Chuan, R.D. Cadle, and D.C. Woods, Small particles in volcanic eruption clouds, *Am. J. Sci.*, *280*, 671-696, 1980.

Sawada, Y., Study on analysis of volcanic eruptions based on eruption cloud image data obtained by the geostationary Meteorological Satellite (GMS), *Tech. Rep. Meteorol. Res. Inst. Jpn.*, *22*, 1987.

Schneider, D.J., and W.I Rose, Observations of the 1989-90 Redoubt Volcano eruption clouds using AVHRR satellite imagery, in *U.S. Geol. Surv. Bull.*, *2047*, in press, 1993.

Schneider, D.J., W.I. Rose, and L. Kelley, Real time tracking of 1992 Crater Peak/Spurr eruption clouds using AVHRR, U.S. Geol. Surv. Bull., in press, 1994.

Shettle, E.P., and J.A. Weinman, The transfer of solar irradiance through inhomogeneous turbid atmospheres evaluated by Eddington's Approximation, *J. Atmos. Sci.*, *47*, 1048-1055, 1970.

Tabazadeh, A., and R.P. Turco, Stratospheric chlorine injection by volcanic eruptions: HC1 scavenging and implications for ozone, *Science*, *260*, 1082-1086, 1993.

Turco, R.P., O.B. Toon, R.C. Whitten, P. Hamill, and R.G. Keesee, The 1980 eruptions of Mount St. Helens: Physical and chemical processes in the stratospheric clouds, *J. Geophys. Res.*, *88*, 5299-5319, 1983.

Volz, F.E., Infrared optical constants of ammonium sulfate, Sahara dust, volcanic pumice, and flyash, *Appl. Opt.*, *12*(3), 564-568, 1973.

Wu, M.L., A method for remote sensing the emissivity, fractional cloud cover and cloud top temperature of high-level, thin clouds. *J. Clim. Appl. Meteorol.*, *26*(2), 225-233, 1987.

Yamanouchi, T., K. Suzuki, and S. Kawaguchi, Detection of clouds in Antarctica from infrared multispectral data of AVHRR, *J. Meteorol. Sci. Jpn.*, *65*(6), 949-962, 1987.

W. I. Rose and S. Wen, Department of Geological Engineering, Geology and Geophysics, Michigan Technological University, Houghton, MI 49931. (e-mail: raman@mtu.edu; shwen@mtu.edu)